ChemPubSoc Europe

DOI: 10.1002/chem.201403714

CHEMISTRY
A European Journal
Full Paper

Template Synthesis

Vernier-Templated Synthesis, Crystal Structure, and Supramolecular Chemistry of a 12-Porphyrin Nanoring

Dmitry V. Kondratuk,[a] Johannes K. Sprafke,[a] Melanie C. O'Sullivan,[a] Luis M. A. Perdigao,[b] Alex Saywell,[b] Marc Malfois,[c] James N. O'Shea,[b] Peter H. Beton,[b] Amber L. Thompson,*[a] and Harry L. Anderson*[a]

Abstract: Vernier templating exploits a mismatch between the number of binding sites in a template and a reactant to direct the formation of a product that is large enough to bind several template units. Here, we present a detailed study of the Vernier-templated synthesis of a 12-porphyrin nanoring. NMR and small-angle X-ray scattering (SAXS) analyses show that Vernier complexes are formed as intermediates in the cyclo-oligomerization reaction. UV/Vis/NIR titrations show that the three-component assembly of the 12-porphyrin nanoring figure-of-eight template complex displays high allosteric cooperativity and chelate cooperativity. This nanoring–template 1:2 complex is among the largest synthetic molecules to have been characterized by single-crystal analysis. It crystallizes as a racemate, with an angle of 27° between the planes of the two template units. The crystal structure reveals many unexpected intramolecular C–H···N contacts involving the *tert*-butyl side chains. Scanning tunneling microscopy (STM) experiments show that molecules of the 12-porphyrin template complex can remain intact on the gold surface, although the majority of the material unfolds into the free nanoring during electrospray deposition.

Introduction

Ever since Sondheimer's seminal work on annulenes,[1] macrocycles with π-conjugated perimeters have provided fascinating systems for testing theories of molecular electronic structure. Recently, the invention of synthetic routes to very large π-conjugated macrocycles has sparked a renaissance in this field, driven by the quest to understand energy transfer, charge delocalization, and nonlinear optical phenomena in these nanostructures.[2–15] Template-directed synthesis makes it possible to create large, fully π-conjugated macrocycles in a size-range that could not have been reached without programmed self-assembly.[7,9,10] The classical template effect translates information from the size and shape of a template to direct the construction of a complementary macrocycle.[16] We have used this approach to prepare nanorings consisting of 6 and 8 porphyrin units, using hexadentate and octadentate templates.[9a–c] This classical approach is not convenient for the synthesis of larger nanorings because of the inaccessibility of suitable templates.

Vernier complexes are formed between a host and a guest when the number of binding sites on one component is not an integer multiple of the number of binding sites on the other component. Self-assembly generates a structure with a number of binding sites that is the lowest common multiple of the numbers of sites on the host and the guest.[17] Recently, we demonstrated that the Vernier effect can be exploited to direct the synthesis of large nanorings using small templates.[9d,e] In effect, the size of the template can be amplified if the number of binding sites on the template is not a multiple of the number of binding sites on the building block. This concept was first illustrated by the synthesis of a 12-porphyrin nanoring ***c*-P12** by coupling a linear porphyrin tetramer ***l*-P4** in the presence of a hexadentate template **T6** (Scheme 1).[9d] Here, we present a full account of the synthesis, crystal structure, and template-binding behavior of ***c*-P12**, including an investigation into the mechanism of Vernier templating. Small-angle X-ray scattering (SAXS) and NMR spectroscopic analysis provide evidence for the formation of the Vernier complex $(\mathbf{\textit{l}\text{-}P4})_3{\cdot}(\mathbf{T6})_2$ under the conditions of the template-directed synthesis. UV/Vis/NIR titrations show that folding of ***c*-P12** into the

[a] Dr. D. V. Kondratuk, Dr. J. K. Sprafke, Dr. M. C. O'Sullivan, Dr. A. L. Thompson, Prof. H. L. Anderson
Department of Chemistry
University of Oxford
Chemistry Research Laboratory
Oxford, OX1 3TA (UK)
E-mail: amber.thompson@chem.ox.ac.uk
harry.anderson@chem.ox.ac.uk

[b] Dr. L. M. A. Perdigao, Dr. A. Saywell, Prof. J. N. O'Shea, Prof. P. H. Beton
School of Physics & Astronomy
University of Nottingham
Nottingham, NG7 2RD (UK)

[c] Dr. M. Malfois
Diamond Light Source Ltd.
Harwell Science and Innovation Campus
Didcot, OX11 0DE (UK)

Supporting information for this article is available on the WWW under http://dx.doi.org/10.1002/chem.201403714.

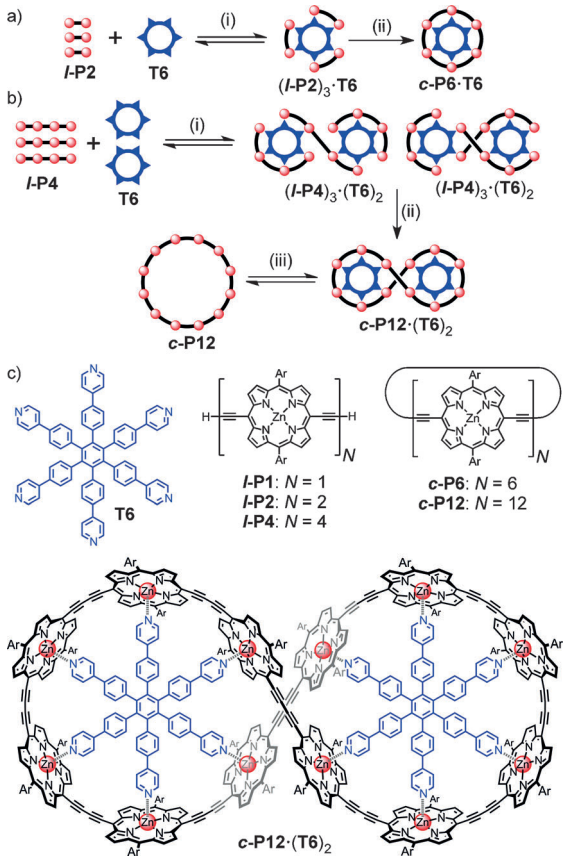

Scheme 1. a) Classical template-directed synthesis of ***c*-P6.** b) Vernier-templated synthesis of ***c*-P12**: (i) self-assembly; (ii) $[PdCl_2(PPh_3)_2]$, CuI, benzoquinone, iPr_2NH; (iii) pyridine. c) Chemical structures; Ar = 3,5-bis(*tert*-butyl)-phenyl or 3,5-bis(octyloxy)phenyl, as indicated by the subscript "*t*Bu" or "C8", respectively.

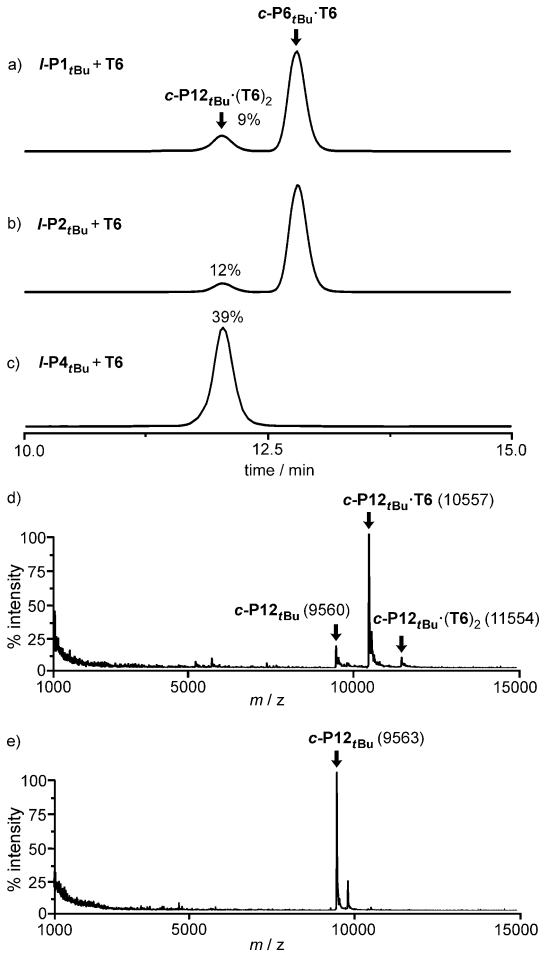

Figure 1. Analytical GPC traces (THF, detection at 360 nm) of the crude reaction mixtures of coupling a) ***l*-P1$_{tBu}$**, b) ***l*-P2$_{tBu}$**, and c) ***l*-P4$_{tBu}$** in the presence of **T6** and the corresponding analytical yields. The analytical yields shown were determined by comparing the areas of ***c*-P12$_{tBu}$·(T6)$_2$** with the area of standard injection of ***c*-P12$_{tBu}$·(T6)$_2$**. Before GPC analysis, the coupling reagents (the catalysts and 1,4-benzoquinone) and insoluble polymers were removed by passing through a short alumina column in $CHCl_3$. MALDI-TOF spectra of d) ***c*-P12$_{tBu}$·(T6)$_2$** and e) ***c*-P12$_{tBu}$**.

figure-of-eight template complex ***c*-P12·(T6)$_2$** is a highly cooperative process. Here, we report the crystal structure of ***c*-P12·(T6)$_2$**, which is the largest porphyrin oligomer yet to have been characterized by single-crystal X-ray analysis. Scanning tunneling microscopy (STM) was also used to image ***c*-P12** and ***c*-P12·(T6)$_2$** molecules on a gold surface.

Results and Discussion

Synthesis of *c*-P12

During our initial work on the synthesis of the cyclic porphyrin hexamer ***c*-P6$_{tBu}$**, by palladium-catalyzed oxidative coupling of the linear porphyrin monomer ***l*-P1$_{tBu}$** or dimer ***l*-P2$_{tBu}$** in the presence of the hexapyridyl template **T6** (Scheme 1a), we noticed the formation of a high-mass byproduct, which was identified as the 12-porphyrin nanoring figure-of-eight complex ***c*-P12$_{tBu}$·(T6)$_2$**.[9b,c] Analytical gel permeation chromatography (GPC) analysis of crude reaction mixtures (Figure 1 a,b) indicated that ***c*-P12$_{tBu}$·(T6)$_2$** was formed in yields of 9 and 12% from ***l*-P1$_{tBu}$** and ***l*-P2$_{tBu}$**, respectively. The mass spectrum of ***c*-P12$_{tBu}$·(T6)$_2$** (MALDI-TOF MS; Figure 1 d) reveals a molecular ion at twice the molecular weight of ***c*-P6$_{tBu}$·T6**, as well as peaks related to loss of one or two template units. Treatment with pyridine, gave the free nanoring ***c*-P12$_{tBu}$**, which was thoroughly characterized by ^{1}H NMR spectroscopy and MALDI-TOF MS analysis (Figure 1 e).[9d]

These serendipitous syntheses of the 12-ring ***c*-P12$_{tBu}$** from porphyrin monomer and dimer indicated that a porphyrin tetramer starting material ***l*-P4$_{tBu}$** would give the 12-ring as the main product, because the 6-ring ***c*-P6$_{tBu}$** could not be formed in this case. We conjectured that a Vernier complex ***(l*-P4$_{tBu}$)$_3$·(T6)$_2$** might form directly from the starting materials and lead to efficient formation of the figure-of-eight complex ***c*-P12$_{tBu}$·(T6)$_2$** (Scheme 1b). Alternatively, oligomerization of the unbound porphyrin tetramer and subsequent cyclization around two, four, six etc. template molecules should form the series of macrocycles ***c*-P*N*** with ***N*** being a multiple of twelve. In general, the coupling of a starting material with *x* binding sites in the presence of a suitable template with *y* binding

sites should lead to formation of a macrocycle with *z* binding sites, where *z* is lowest common multiple of *x* and *y*.

As expected, palladium-catalyzed oxidative coupling of the linear porphyrin tetramer ***l*-P4$_{tBu}$** in the presence of **T6** gave the figure-of-eight complex ***c*-P12$_{tBu}$·(T6)$_2$** as the major product in 39% isolated yield (Figure 1c).[9d] The only other products of this reaction were insoluble polymers and traces of high-mass oligomers, which were difficult to isolate due to their low solubility. To learn more about this reaction, we investigated the coupling of porphyrin tetramer bearing octyloxy side chains ***l*-P4$_{C8}$**, as a means to improve the solubility of cyclic byproducts.

Coupling of the linear porphyrin tetramer ***l*-P4$_{C8}$** in the presence of template **T6** at various mole ratios (***l*-P4$_{C8}$:T6**) gave mixtures of cyclic and linear oligomers, all as complexes with the **T6** template. The linear polymers were removed by using a short alumina column, and the template was removed by addition of pyridine, prior to GPC analysis (Figure 2). In all cases studied (***l*-P4$_{C8}$/T6** = 1.0, 1.5, 3.0), the major product was ***c*-P12$_{C8}$**. Formation of the 12-ring is most efficient when using a stoichiometric amount of template (***l*-P4$_{C8}$/T6** = 1.5). However, ***c*-P12$_{C8}$** was never the only product and traces of smaller (***c*-P8$_{C8}$**) and larger (e.g., ***c*-P16$_{C8}$** and ***c*-24$_{C8}$**) cyclic species were detected. None of these cyclic oligomers formed in the absence of a template.

In keeping with the GPC analysis, ***c*-P12$_{C8}$** was isolated in 32% yield by using a stoichiometric amount of **T6**. This yield is comparable to the isolated yield obtained from the Vernier synthesis of ***c*-P12$_{tBu}$** (39%). With a 1:1 mole ratio of ***l*-P4$_{C8}$:T6**, the yield of ***c*-P12$_{C8}$** decreased to 16%, and ***c*-P16$_{C8}$** was isolated in 6% yield.

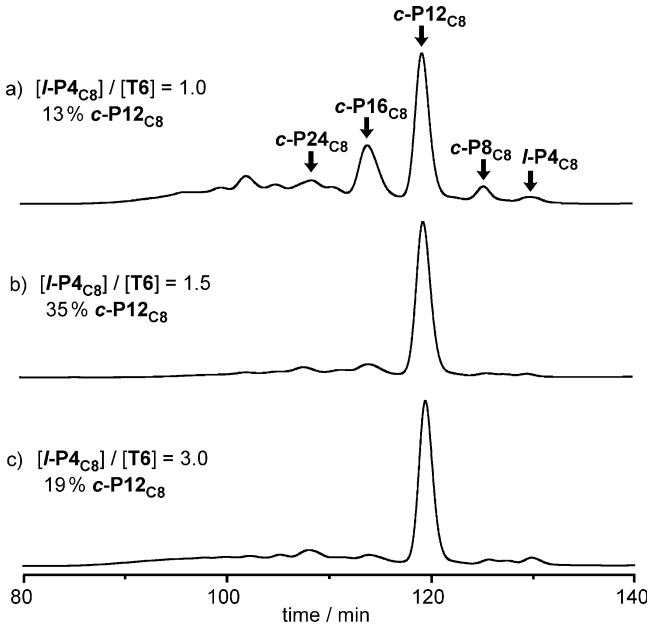

Figure 2. Recycling GPC traces (2nd cycle shown, toluene/1% pyridine, detection at 500 nm) of the crude reaction mixtures of coupling ***l*-P4$_{C8}$** in the presence of **T6** at various ***l*-P4$_{C8}$/T6** ratios and the corresponding analytical yields of ***c*-P12$_{C8}$**. The analytical yields were determined by comparing the areas of ***c*-P12$_{C8}$** with the area of standard injection of ***c*-P12$_{C8}$**. The coupling reagents (the catalysts and 1,4-benzoquinone) and **T6** were removed by passing through a short alumina column in $CHCl_3$ and a size-exclusion column in $CHCl_3$/10% pyridine, respectively.

Probing the Mechanism of Vernier Templating

In principle, Vernier templated coupling of a starting material ***l*-P*x*** with *x* binding sites in the presence of a template **T*y*** to give a product ***c*-P*z*** (where *z* is the lowest common multiple of *x* and *y*) could operate through two mechanisms: 1) the template waits until oligomerization has generated a linear species ***l*-P*z***, at which point it binds strongly to form a complex ***l*-P*z*·(T*y*)$_{z/y}$**, which then undergoes rapid coupling to give ***c*-P*z*·(T*y*)$_{z/y}$**, or 2) a Vernier complex **(*l*-P*x*)$_{z/x}$·(T*y*)$_{z/y}$** is formed, which then couples to give ***c*-P*z*·(T*y*)$_{z/y}$**. In practice, the reaction could proceed by a combination of these extremes, with coupling of both free and bound oligomers. We decided to test whether ***l*-P4$_{tBu}$** coordinates to **T6** to form a stable Vernier complex **(*l*-P4)$_3$·(T6)$_2$** under the conditions of the reaction (toluene solution, 20 °C), to establish whether this complex is a plausible intermediate.

A ^{1}H NMR titration of ***l*-P4$_{C8}$** with **T6** (500 MHz, $CDCl_3$, 298 K) showed only broadening of the initial spectrum of ***l*-P4$_{C8}$** and no useful structural information could be extracted. To assess the size of the complex, we used diffusion-ordered NMR spectroscopy (DOSY).[18] The 2D DOSY spectrum of a 3:2 mixture of ***l*-P4$_{C8}$** and **T6** shows similar diffusion coefficients for porphyrin and template signals, thereby confirming that both components bind together to form a complex (Figure S3). The diffusion coefficient of this complex ($D = 1.92 \pm 0.14 \times 10^{-10}$ m^2 s^{-1}) is the same as that of the figure-of-eight ***c*-P12$_{C8}$·(T6)$_2$** complex ($D = 1.91 \pm 0.07 \times 10^{-10}$ m^2 s^{-1}), strongly supporting the formation of a Vernier complex **(*l*-P4$_{C8}$)$_3$·(T6)$_2$**. The diffusion coefficients of ***c*-P12$_{C8}$·(T6)$_2$** and **(*l*-P4$_{C8}$)$_3$·(T6)$_2$** are significantly smaller than those of ***l*-P4$_{C8}$** ($D = 2.52 \pm 0.04 \times 10^{-10}$ m^2 s^{-1}) and **T6** ($D = 5.34 \pm 0.25 \times 10^{-10}$ m^2 s^{-1}) and slightly bigger than that of ***c*-P12$_{C8}$** ($D = 1.58 \pm 0.04 \times 10^{-10}$ m^2 s^{-1}), all measured at 298 K in $CDCl_3$ (with 1% d_5-pyridine to prevent aggregation in the case of ***l*-P4$_{C8}$** and ***c*-P12$_{C8}$**).

We also analyzed the size and shape of these complexes by using solution-phase small-angle X-ray scattering (SAXS).[19,20] SAXS data for ***c*-P12$_{tBu}$·(T6)$_2$** and ***c*-P12$_{tBu}$** in toluene match the simulated pair-distribution functions (PDF) for geometries from molecular mechanics calculations (Figure 3a,b). The PDF $p(r)$ represents the probability of finding electron density at separation *r*. In contrast to the template complex, the free nanoring ***c*-P12$_{tBu}$** is flexible in solution and its SAXS data could only be adequately simulated by using a combination of several elliptical conformations.[9d] The average of the scattering curves from six models is in excellent agreement with the experimental scattering data (Figure 4b). The Guinier fits[21] calculated from the experimental scattering data for **(*l*-P4$_{tBu}$)$_3$·(T6)$_2$** are linear in the low-Q region, confirming that the system is monodisperse (Figure 4c insert). The PDF of **(*l*-P4$_{tBu}$)$_3$·(T6)$_2$** matches well with the simulated curve, and is similar to that of ***c*-P12$_{tBu}$·(T6)$_2$**; the peaks at around 23 and 50 Å correspond to the dimensions from molecular mechanics calculations. The broad PDF func-

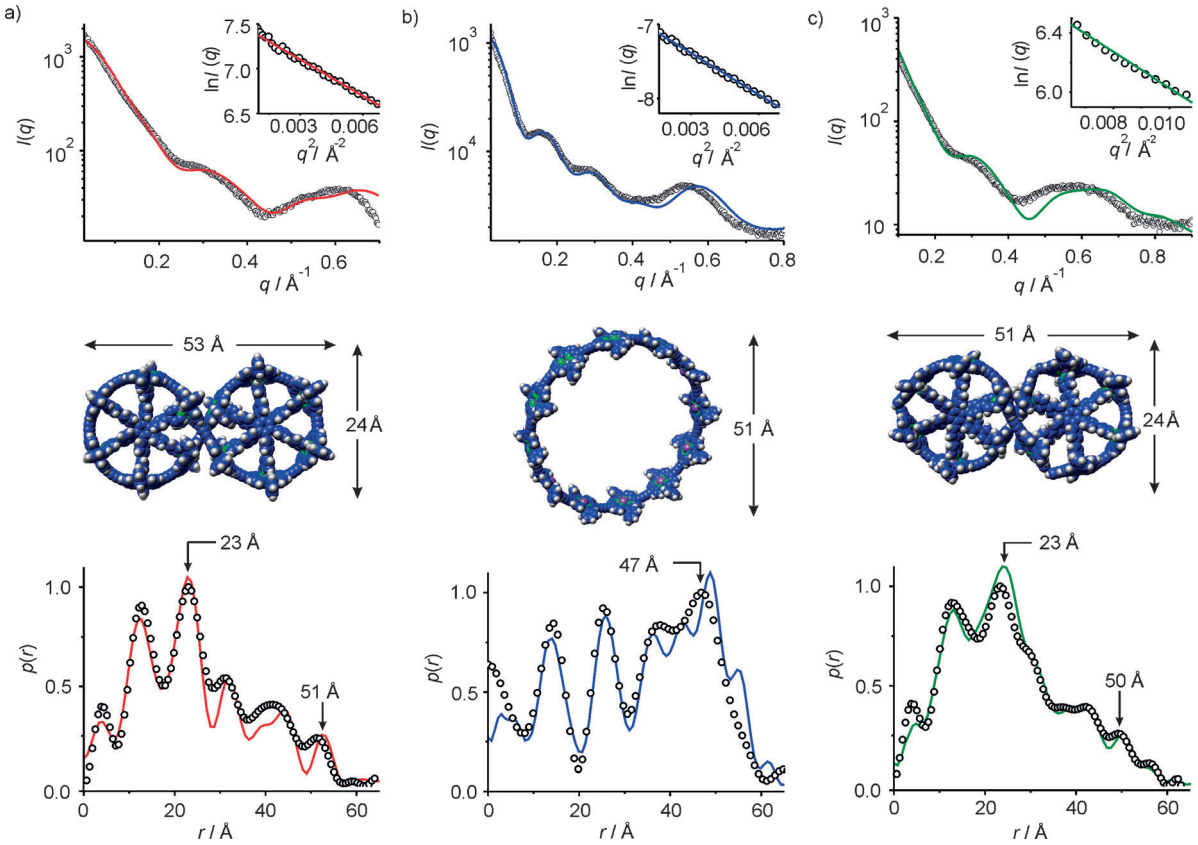

Figure 3. SAXS analysis of a) figure-of-eight complex ***c*-P12$_{tBu}$·(T6)$_2$** in toluene, b) cyclic dodecamer ***c*-P12$_{tBu}$** in toluene/1% pyridine, and c) Vernier complex (***l*-P4$_{tBu}$)$_3$·(T6)$_2$** in toluene (298 K). The top row shows the experimental scattering data (black circles) together with the simulated curves based on calculated models (solid lines) calculated from the experimental scattering data and the radii of gyration R_g. The bottom row shows pair-distribution functions determined experimentally (black circles) and from models (solid lines).

tion of (***l*-P4$_{tBu}$)$_3$·(T6)$_2$** reflects its less regular shape compared with ***c*-P12$_{tBu}$·(T6)$_2$**. The radii of gyration R_g determined for the three structures from the Guinier fit[21] are in good agreement with the values from molecular mechanic calculations (Table 1; MM$^+$ force field, HyperChem^{TM}).

Crystal Structure of *c*-P12$_{tBu}$·(T6)$_2$[22]

The three-dimensional structure of ***c*-P12$_{tBu}$·(T6)$_2$** was initially deduced from a detailed analysis of the ^{1}H NMR and SAXS data.[9d] Crystals of ***c*-P12$_{tBu}$·(T6)$_2$** were grown by slow diffusion of methanol vapor into a solution of ***c*-P12$_{tBu}$·(T6)$_2$** in $CHCl_3$ over a period of several days. The best diffraction data were obtained from freshly grown crystals. The crystals contained over 60% solvent by volume, resulting in weak diffraction. They were assigned to the *C*2/*c* space group with a cell of $a=117.44(5)$ Å, $b=21.009(7)$ Å, $c=57.23(2)$ Å, $\alpha=90^\circ$, $\beta=115.385(4)^\circ$, $\gamma=90^\circ$, $V=127{,}561$ Å^3. The asymmetric unit contains six porphyrin units (labeled A–F in Figure 4a), that is, half a molecule of ***c*-P12$_{tBu}$·(T6)$_2$**, with a C_2 axis bisecting the molecule at the cross-point of central butadiyne moieties. The distance between the centroids of the two central butadiyne units (along the C_2 axis of the molecule) is 4.24(2) Å and the shortest C···C distance between the central carbon atoms is 4.31(2) Å, which is too long for direct van der Waals contact. The torsion angle between these two butadiyne moieties (measured *meso*-centroid-centroid-*meso*) is 74°. This arrangement of the butadiynes is clearly unsuitable for topochemical reaction.[23] There are eight short C–H···N contacts across the central groove of the figure-of-eight, between porphyrins A and F, between *tert*-butyl protons and pyrrole nitrogen atoms (Figure 4d, H···N distances: 3.17–3.32(2) Å; C···N distances 3.78–4.08(13) Å; C–H···N angles: 118–144°). These distances are too long for a classical C–H···N hydrogen bond,[24] and they can be classified as C–H···π(N) interactions.[25] The distances between the hydrogen atoms to the mean plane of the porphyrin are 2.893–4.00(9) Å. These contacts probably make an insignificant contribution to the energy of the figure-of-eight conformation, but they account for the unusual chemical shift observed for these *tert*-butyl protons ($\delta_H=-0.64$ ppm in $CDCl_3$ solution)[9d] and they may explain why the yield for Vernier synthesis of ***c*-P12$_{C8}$·(T6)$_2$** is lower than that for the synthesis of ***c*-P12$_{tBu}$·(T6)$_2$**. It is easy to see how this type of interaction could become destabilizing when the *t*Bu substituents are changed to larger solubilizing groups.

In the crystal, each molecule of ***c*-P12$_{tBu}$·(T6)$_2$** has C_2 symmetry, with approximate D_2 symmetry. The symmetry in solution is D_2. Both the C_2 and D_2 point groups are chiral, however, the compound crystallizes as a racemate, and each enantiomer constitutes a separate flat layer in which molecules are stacked

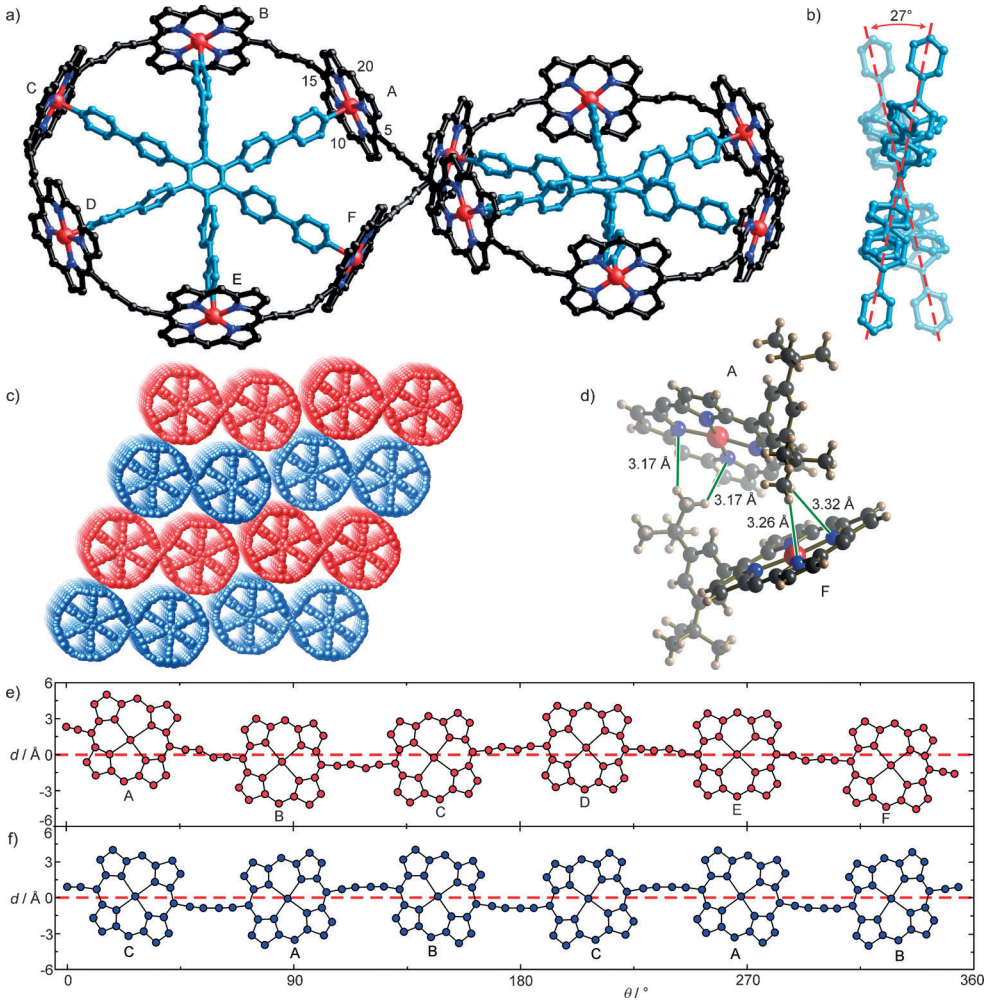

Figure 4. a) Solid-state structure of ***c*-P12$_{tBu}$·(T6)$_2$**; hydrogen atoms, aryl groups, and solvent molecules are omitted for clarity. The asymmetric unit contains six porphyrins labeled A–F. b) View showing the 27° twist between the mean planes of the two templates. c) Packing diagram with the two enantiomers of ***c*-P12$_{tBu}$·(T6)$_2$** shown in red and blue. d) View of the C–H···N contacts between porphyrin units A and F across the external grooves the center of the figure-of-eight. (e and f) Radial projections of porphyrin cores and connecting 1,3-butadiyne linkers in the crystal structures of templated complexes ***c*-P12$_{tBu}$·(T6)$_2$** (e) and ***c*-P12$_{tBu}$·T6** (f), where d is the distance of each atom from the mean plane of the six zinc atoms; θ is the angle projected onto this mean plane (see the Supporting Information for detailed description of the construction of these radial plots).

Table 1. Comparison of experimentally determined and calculated radii of gyration R_g.

Compound	R_g (exp, SAXS) [Å]	R_g (calc) [Å]
***c*-P12$_{tBu}$·(T6)$_2$**	20.1	18.2
***c*-P12$_{tBu}$**	23.7	24.8
(***l*-P4$_{tBu}$**)$_3$·(T6)$_2$	19.0	18.4

side-to-side (Figure 4c). The angle between the mean planes of the two template units is 27° (Figure 4b).

Comparison of the structures of ***c*-P6$_{tBu}$·T6**[9c] and ***c*-P12$_{tBu}$·(T6)$_2$** shows that the figure-of-eight topology does not change the size of the six-porphyrin loop. The mean Zn···Zn diameter appears to be fixed by the template: 24.35(8) Å in ***c*-P6$_{tBu}$·T6** vs. 24.36(5) Å in ***c*-P12$_{tBu}$·(T6)$_2$**. In contrast, locking two six-porphyrin loops into a figure-of-eight alters the out-of-plane geometry, as shown by the radial projections of the porphyrin cores and 1,3-butadiyne units onto the mean plane of the six zinc centers (Figure 4e). In the case of ***c*-P6$_{tBu}$·T6**, the seamless six-porphyrin ring ruffles to adopt a "chair-like" conformation (Figure 4f),[9c] with alternate butadiynes above and below the plane of the six zinc centers. This chair-conformation only partially persists in the six-porphyrin loop of ***c*-P12$_{tBu}$·(T6)$_2$**. Unfortunately, the low resolution of the diffraction data does not allow us to reliably analyze the zinc to pyridine nitrogen bond lengths or bond-length alternation in the 1,3-butadiyne units.

STM Imaging of *c*-P12$_{C8}$ and *c*-P12$_{C8}$·(T6)$_2$

Scanning tunneling microscopy (STM) provides an alternative way to evaluate the structure of ***c*-P12$_{C8}$** and ***c*-P12$_{C8}$·(T6)$_2$** (Figure 5). Molecules were deposited by using an electrospray source, on a Au(111) surface under ultrahigh vacuum, at room temperature, using solutions of the compounds in toluene containing MeOH (5% by volume).[26] The sample of ***c*-P12$_{C8}$** used in these experiments was synthesized from ***l*-P4$_{C8}$** (as described above) without extensive GPC purification and it contained impurities of other cyclic species. The STM images of ***c*-P12$_{C8}$** showed the presence of many porphyrin nanorings with clearly defined twelve-porphyrin units (Figure 5a,b). However, the presence of some ***c*-P16$_{C8}$** was also detected. We attempted to image the ***c*-P12$_{C8}$·(T6)$_2$** complex by applying the same imaging conditions used for ***c*-P12$_{C8}$** (Figure 5c). Most of the molecules are evident in the form of unfolded ***c*-P12$_{C8}$**, and the images showed the presence of few intact molecules of ***c*-P12$_{C8}$·(T6)$_2$** with clearly defined six-porphyrin loops approximately 2 nm in diameter, consistent with the calculated value of approximately 2 nm. In the case of ***c*-P12$_{C8}$**, the molecules lie flat on the surface, similar to previously reported STM imaging experiments performed on linear porphyrin oligomers.[26] In contrast, mole-

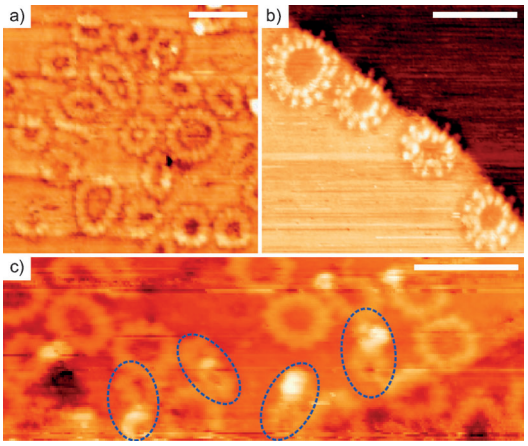

Figure 5. STM imaging of nanorings on a Au(111) surface under UHV. Scale bars: 10 nm. Images a) and b) show samples of ***c*-P12$_{C8}$** with some ***c*-P16$_{C8}$** impurity. c) ***c*-P12$_{C8}$·(T6)$_2$**; most of the molecules of the complex unfold into the free ***c*-P12$_{C8}$** during deposition but some intact ***c*-P12$_{C8}$·(T6)$_2$** units are indicated by blue dashed ellipses.

cules of ***c*-P12$_{C8}$·(T6)$_2$** should have the planes of their individual porphyrin units set perpendicular to the gold surface.

Thermodynamics of Binding of T6 by *c*-P12$_{tBu}$

When the flexible free nanoring ***c*-P12$_{tBu}$** binds the **T6** template to form the compact figure-of-eight complex, there is a decrease in the radius of gyration (Table 1) and an increase in the diffusion coefficient (see Figure S3), which are characteristics of a folding event. The cooperativity of this binding process is reminiscent of protein folding. Formation of the 1:2 figure-of-eight ***c*-P12$_{tBu}$·(T6)$_2$** must occur through the formation of a 1:1 complex ***c*-P12$_{tBu}$·T6** (Figure 6a). The equilibrium constants of the two events are linked by the interaction parameter α, which quantifies the allosteric cooperativity between the binding of the two templates; if $\alpha = 1$ then binding of the two **T6** molecules is statistical, if $\alpha \gg 1$ there is strong positive cooperativity between the two binding events and the intermediate complex ***c*-P12$_{tBu}$·T6** is not significantly populated. In terms of the allosteric cooperativity between the two template molecules, one would expect the energetic cost of nanoring folding to be mostly paid after the first template is bound. Binding of the second template should be favored because of the preorganization of the binding pocket, giving an interaction parameter α greater than 1. This picture of a process with high chelate as well as allosteric cooperativity was confirmed by a ^{1}H NMR titration of **T6** into ***c*-P12$_{tBu}$**. A clear transition occurs from the spectrum of ***c*-P12$_{tBu}$** to that of the figure-of-eight ***c*-P12$_{tBu}$·(T6)$_2$** without any detectable intermediate species. Figure 7 shows the alkyl region of the spectra, which is dominated by the *tert*-butyl singlet at $\delta_H = 1.56$ ppm in ***c*-P12$_{tBu}$**. This resonance evolves cleanly into the various *tert*-butyl signals characteristic of the figure-of-eight ***c*-P12$_{tBu}$·(T6)$_2$** complex, without showing any sign of a 1:1 intermediate (although this 1:1 complex is observed by MALDI-TOF MS; Figure 1d).

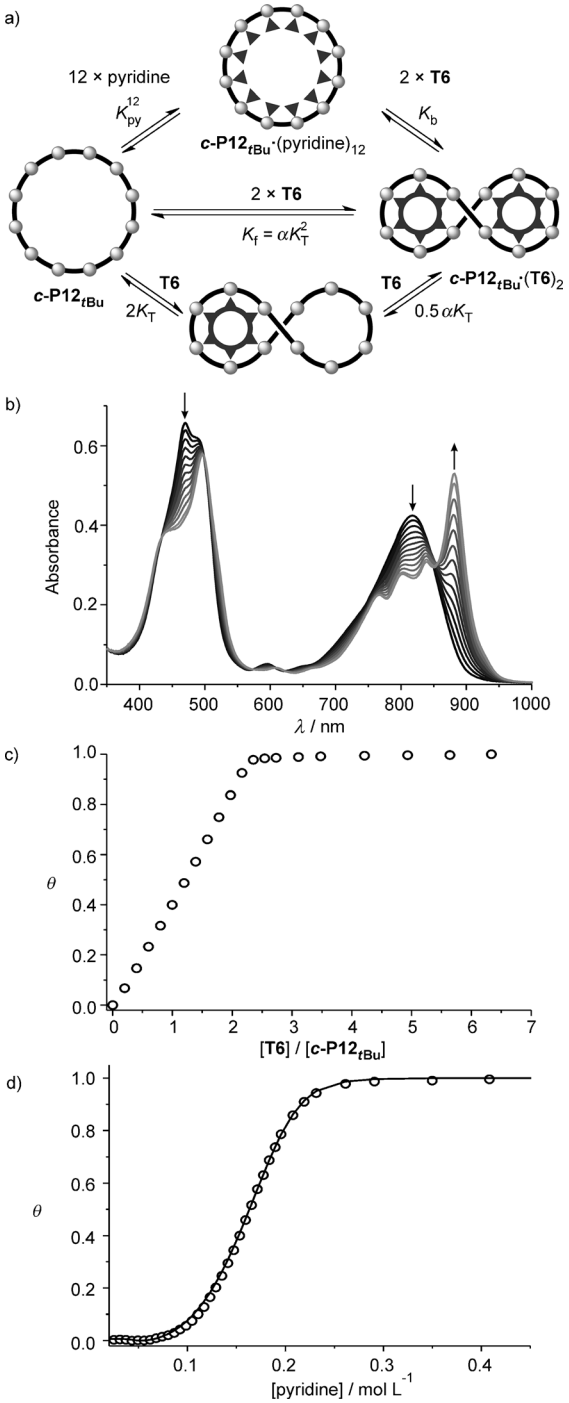

Figure 6. a) Simplified equilibria for the formation of the figure-of-eight complex **(*c*-P12$_{tBu}$)·(T6)$_2$** from ***c*-P12$_{tBu}$** and break-up with pyridine. b) Changes in absorption upon addition of **T6** to ***c*-P12$_{tBu}$** ([***c*-P12$_{tBu}$**] = 4.4×10^{-7} M, $CHCl_3$, 298 K), and c) fraction of formed ***c*-P12$_{tBu}$·(T6)$_2$** from the difference in absorption ΔA at 882–812 nm plotted against the ratio **T6**/***c*-P12$_{tBu}$**. A small amount of pyridine ([pyridine] = 6.2×10^{-7} M) was added at the beginning of the titration to disaggregate ***c*-P12$_{tBu}$**. d) Binding isotherm (black circles) ([***c*-P12$_{tBu}$·(T6)$_2$**] = 5.2×10^{-7} M) derived from absorption data at 883 nm and calculated fit.

The clean all-or-nothing equilibrium between ***c*-P12$_{tBu}$** and ***c*-P12$_{tBu}$·(T6)$_2$** is also observed at submicromolar concentrations by UV/Vis/NIR titration (Figure 6b,c). The observation of several

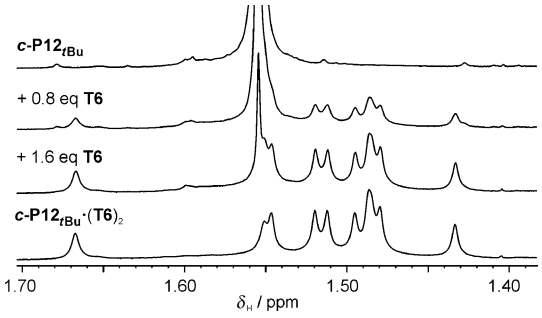

Figure 7. ^{1}H NMR titration of ***c*-P12$_{tBu}$** ([***c*-P12$_{tBu}$**] = 3.6×10^{-4} M in $CDCl_3$, 500 MHz, 298 K) with **T6** in $CDCl_3$/3% MeOD. [**T6**] increases downwards.

isosbestic points indicates the presence of only two absorbing species: the free nanoring and the figure-of-eight complex. The binding isotherm is square and reaches saturation after addition of two equivalents of **T6**, corresponding to the stoichiometry of ***c*-P12$_{tBu}$·(T6)**. To quantify the 1:2 cooperativity, it was necessary to first determine the formation constant of the figure-of-eight complex K_f. However, the squareness of the binding isotherm prevents the direct determination of K_f by means of a formation titration.

Large equilibrium constants can be determined indirectly by competition experiments, as illustrated by the thermodynamic cycle in Figure 6a.[9a,b,27] Addition of an excess of the competing ligand pyridine to ***c*-P12$_{tBu}$·(T6)$_2$** will result in displacement of the template molecules and formation of the pyridine complex ***c*-P12$_{tBu}$·(pyridine)$_{12}$**. The equilibrium constant for this break-up process K_b and the binding constant of pyridine to ***c*-P12$_{tBu}$** K_{py} can be used to calculate K_f using Equation (1):

$$K_t = \frac{K_{py}^{12}}{K_b} \quad (1)$$

The binding constant of pyridine with ***c*-P12$_{tBu}$** is difficult to measure because ***c*-P12$_{tBu}$** aggregates in the absence of pyridine. The association constant of pyridine with porphyrin monomer ***l*-P1$_{tBu}$** is expected to be very similar to that with ***c*-P12$_{tBu}$** and is therefore used as K_{py} ($K_{py} = 1.0\pm0.1\times10^4$ M^{-1}).[9a,b,27] A large excess of pyridine (ca. 500,000 equivalents) is necessary to completely displace the templates from ***c*-P12$_{tBu}$·(T6)$_2$** at the concentration of a UV/Vis/NIR titration (Figure 6d). The presence of several isosbestic points (Figure S4) confirms the expected two-state equilibrium, and the sigmoidal binding curve indicates high cooperativity. The equilibrium constant ($K_b = 7.9\pm0.8\times10^{-4}$ M^{-10}) was determined by fitting the binding isotherm at 883 nm using the program SPECFIT, and the resulting formation constant of the figure-of-eight complex K_f was 1.8×10^{51} M^{-2}. The uncertainty in this number is high because of the error propagation in K_{py}^{12} and the value is thus given as log $K_f = 51.3\pm0.6$.

As shown in Figure 6a, the formation constant of the figure-of-eight complex K_f can be expressed by the binding constant of one template K_T and the interaction parameter α accounting for the allosteric cooperativity [Eq. (2)]:

$$K_f = \alpha K_T^2 \quad (2)$$

K_T depends on the binding constant of one arm of the template K_1 and the average effective molarity *EM* that quantifies the chelate cooperativity [Eq. (3)]:

$$K_T = EM^5 K_1^6 \quad (3)$$

From Equations (2) and (3), the combined allosteric and chelate cooperativity in the formation of the figure-of-eight complex is given by Equation (4):

$$\sqrt[10]{\alpha}EM = \sqrt[10]{\frac{K_f}{K_1^{12}}} \approx EM \quad (4)$$

Since the interaction parameter α contributes only in the 10th root to this overall cooperativity, its effect on the value is negligible and the result will be a good approximation of the average effective molarity *EM*.[27] The binding constant of one arm of the template to ***c*-P12$_{tBu}$** K_1 can be approximated from the binding constant of 4-(phenyl)pyridine to porphyrin monomer ***l*-P1$_{tBu}$**.[9b] With $K_1 = 1.9\pm0.2\times10^4$ M^{-1}, the (statistically uncorrected) average effective molarity of figure-of-eight formation is 1.0 ± 0.2 M. It is remarkable that this high effective molarity is comparable to the value of the cyclic octamer-octadentate template complex ***c*-P8$_{tBu}$·T8** (*EM* = 5.4 M) given that ***c*-P12$_{tBu}$·(T6)$_2$** is a three-component assembly and it is significantly more strained. Presumably the first five *EM*s are relatively low because they are associated with most of the strain. The next five *EM*s corresponding to the binding of the second template are probably significantly higher and similar to the values measured for ligand binding in ***c*-P6$_{tBu}$**.[27] The allosteric cooperativity between the two templates originates from the higher effective molarities of the second template.

Conclusion

The work presented here led to the concept of Vernier template directed synthesis, which appears to be a widely applicable strategy for the preparation of large macrocycles using small, readily available templates.[9e] Our results shed some light on the mechanism of Vernier templating by showing that a Vernier complex (***l*-P4$_{C8}$**)$_3$·(**T6**)$_2$ is formed under the conditions of the coupling reaction.

At first sight, the crystal structure of the figure-of-eight complex ***c*-P12$_{tBu}$·(T6)$_2$** simply confirmed the structure that had already been deduced from NMR and SAXS data. However, on more detailed examination, it revealed several unexpected features, such as the many short C–H···N contacts between the *tert*-butyl group of one porphyrin and the central nitrogen atoms of another porphyrin unit. The observation of these interactions reminds us that the side chains are not just solubilizing groups, and that they can influence the conformational behavior of these porphyrin wires. The replacement of these favorable C–H···N contacts by unfavorable steric interactions may explain why ***l*-P4$_{C8}$** undergoes Vernier templated synthesis

of ***c*-P12$_{C8}$** less efficiently than the analogous reaction of ***l*-P4$_{tBu}$**. Coupling of ***l*-P4$_{C8}$** in the presence of **T6** generates cyclic byproducts such as ***c*-P8**, ***c*-P16**, and ***c*-P24**, which do not appear to be formed from ***l*-P4$_{tBu}$**. The yields of these byproducts are sensitive to the ***l*-P4$_{C8}$:T6** feed ratio, and formation of ***c*-P12$_{C8}$** is favored by using the ideal 3:2 stoichiometry.

This work illustrates how techniques such as SAXS and STM can play an important role as synthetic supramolecular chemistry moves into the size-domain of protein chemistry. STM is an excellent technique for detecting the presence of larger nanorings, such as ***c*-P16$_{C8}$** and ***c*-P24$_{C8}$**, as impurities in ***c*-P12$_{C8}$**. It was also possible to image the ***c*-P12$_{C8}$·(T6)$_2$** figure-of-eight complex, although there was substantial loss of template during electrospray deposition onto the gold surface.

Finally, the results of ^{1}H NMR and UV/Vis/NIR titrations show that formation of the ***c*-P12$_{tBu}$·(T6)$_2$** from a ***c*-P12$_{tBu}$** is a cooperative all-or-nothing folding process, which occurs without detectable amounts of 1:1 intermediates. The formation constant, K_f, of the figure-of-eight complex is $1.8\times10^{51}\,\text{M}^{-2}$ (log $K_f = 51.3\pm0.6$). It will be interesting to compare the folding processes of larger nanorings such as ***c*-P16$_{C8}$**, ***c*-P18$_{C8}$** and ***c*-P24$_{C8}$**.[9e]

Acknowledgements

We thank Diamond Light Source for a generous award of beam time on I22 and on I19 (MT7768) the Engineering and Physical Sciences Research Council (EPSRC), the European Research Council (grant 320969), the EPSRC mass spectrometry service at Swansea, and the Clarendon Fund of the University of Oxford for support. We thank Dr. Tim D. W. Claridge and Dr. Barbara Odell for recording DOSY spectra.

Keywords: conjugation · macrocycles · porphyrinoids · supramolecular chemistry · template synthesis

[1] F. Sondheimer, *Acc. Chem. Res.* **1972**, *5*, 81 – 91.

[2] a) E. L. Spitler, C. A. Johnson II, M. A. Haley, *Chem. Rev.* **2006**, *106*, 5344 – 5386; b) T. Kawase, H. Kurata, *Chem. Rev.* **2006**, *106*, 5250 – 5273; c) M. Iyoda, J. Yamakawa, M. J. Rahman, *Angew. Chem.* **2011**, *123*, 10708 – 10740; *Angew. Chem. Int. Ed.* **2011**, *50*, 10522 – 10553.

[3] a) T. Kawase, H. R. Darabi, M. Oda, *Angew. Chem.* **1996**, *108*, 2803 – 2805; *Angew. Chem. Int. Ed. Engl.* **1996**, *35*, 2664 – 2666.

[4] a) J. Krömer, I. Rios-Carreras, G. Fuhrmann, C. Musch, M. Wunderlin, T. Debaerdemaeker, E. Mena-Osteritz, P. Bäuerle, *Angew. Chem.* **2000**, *112*, 3623 – 3628; *Angew. Chem. Int. Ed.* **2000**, *39*, 3481 – 3486; b) A. Bhaskar, G. Ramakrishna, K. Hagedorn, O. Varnavski, E. Mena-Osteritz, P. Bäuerle, T. Goodson III, *J. Phys. Chem. B* **2007**, *111*, 946 – 954; c) F. Zhang, G. Götz, H. D. F. Winkler, C. A. Schalley, P. Bäuerle, *Angew. Chem.* **2009**, *121*, 6758 – 6762; *Angew. Chem. Int. Ed.* **2009**, *48*, 6632 – 6635; d) F. Zhang, G. Götz, E. Mena-Osteritz, M. Weil, B. Sarkar, W. Kaim, P. Bäuerle, *Chem. Sci.* **2011**, *2*, 781 – 784.

[5] M. Ohkita, K. Ando, T. Tsuji, *Chem. Commun.* **2001**, 2570 – 2571.

[6] M. Mayor, C. Didschies, *Angew. Chem.* **2003**, *115*, 3284 – 3287; *Angew. Chem. Int. Ed.* **2003**, *42*, 3176 – 3179.

[7] a) S.-H. Jung, W. Pisula, A. Rouhanipour, H. J. Räder, J. Jacob, K. Müllen, *Angew. Chem.* **2006**, *118*, 4801 – 4806; *Angew. Chem. Int. Ed.* **2006**, *45*, 4685 – 4690; b) B. Schmaltz, A. Rouhanipour, H. J. Räder, W. Pisula, K. Müllen, *Angew. Chem.* **2009**, *121*, 734 – 738; *Angew. Chem. Int. Ed.* **2009**, *48*, 720 – 724; c) S. C. Simon, B. Schmaltz, A. Rouhanipour, H. J. Räder, K. Müllen, *Adv. Mater.* **2009**, *21*, 83 – 85; d) F. Schlütter, F. Rossel, M. Kivala, V. Enkelmann, J.-P. Gisselbrecht, P. Ruffieux, R. Fasel, K. Müllen, *J. Am. Chem. Soc.* **2013**, *135*, 4550 – 4557.

[8] a) K. Nakao, M. Nishimura, T. Tamachi, Y. Kuwatani, H. Miyasaka, T. Nishinaga, M. Iyoda, *J. Am. Chem. Soc.* **2006**, *128*, 16740 – 16747; b) M. Williams-Harry, A. Bhaskar, G. Ramakrishna, T. Goodson III, M. Imamura, A. Mawatari, K. Nakao, H. Enozawa, T. Nishinaga, M. Iyoda, *J. Am. Chem. Soc.* **2008**, *130*, 3252 – 3253; c) J. E. Donehue, O. P. Varnavski, R. Cemborski, M. Iyoda, T. Goodson, III, *J. Am. Chem. Soc.* **2011**, *133*, 4819 – 4828.

[9] a) M. Hoffmann, C. J. Wilson, B. Odell, H. L. Anderson, *Angew. Chem.* **2007**, *119*, 3183 – 3186; *Angew. Chem. Int. Ed.* **2007**, *46*, 3122 – 3125; b) M. Hoffmann, J. Kärnbratt, M.-H. Chang, L. M. Herz, B. Albinsson, H. L. Anderson, *Angew. Chem.* **2008**, *120*, 5071 – 5074; *Angew. Chem. Int. Ed.* **2008**, *47*, 4993 – 4996; c) J. K. Sprafke, D. V. Kondratuk, M. Wykes, A. L. Thompson, M. Hoffmann, R. Drevinskas, W. H. Chen, C. K. Yong, J. Kärnbratt, J. E. Bullock, M. Malfois, M. R. Wasielewski, B. Albinsson, L. M. Herz, D. Zigmantas, D. Beljonne, H. L. Anderson, *J. Am. Chem. Soc.* **2011**, *133*, 17262 – 17273; d) M. C. O'Sullivan, J. K. Sprafke, D. V. Kondratuk, C. Rinfray, T. D. Claridge, A. Saywell, M. O. Blunt, J. N. O'Shea, P. H. Beton, M. Malfois, H. L. Anderson, *Nature* **2011**, *469*, 72 – 75; e) D. V. Kondratuk, L. M. A. Perdigao, M. C. O'Sullivan, S. Svatek, G. Smith, J. N. O'Shea, P. H. Beton, H. L. Anderson, *Angew. Chem.* **2012**, *124*, 6800 – 6803; *Angew. Chem. Int. Ed.* **2012**, *51*, 6696 – 6699; f) P. Liu, P. Neuhaus, D. V. Kondratuk, T. S. Balaban, H. L. Anderson, *Angew. Chem. Int. Ed.* **2014**, *53*, in press DOI: 10.1002/anie.201402917.

[10] a) D. Mössinger, J. Hornung, S. Lei, S. De Feyter, S. Höger, *Angew. Chem.* **2007**, *119*, 6926 – 6930; *Angew. Chem. Int. Ed.* **2007**, *46*, 6802 – 6806; b) D. Mössinger, D. Chaudhuri, T. Kudernac, S. Lei, S. De Feyter, J. M. Lupton, S. Höger, *J. Am. Chem. Soc.* **2010**, *132*, 1410 – 1423; c) A. V. Aggarwal, S.-S. Jester, S. M. Taheri, S. Förster, S. Höger, *Chem. Eur. J.* **2013**, *19*, 4480 – 4495; d) A. V. Aggarwal, A. Thiessen, A. Idelson, D. Kalle, D. Würsch, T. Stangl, F. Steiner, S.-S. Jester, J. Vogelsang, S. Höger, J. M. Lupton, *Nat. Chem.* **2013**, *5*, 964 – 970.

[11] a) R. Jasti, J. Bhattacharjee, J. B. Neaton, C. R. Bertozzi, *J. Am. Chem. Soc.* **2008**, *130*, 17646 – 17647. J. Xia, J. W. Bacon, *Chem. Sci.* **2012**, *3*, 3018 – 3021; b) A. V. Zabula, A. S. Filatov, J. Xia, R. Jasti, M. A. Petrukhina, *Angew. Chem.* **2013**, *125*, 5137 – 5140; *Angew. Chem. Int. Ed.* **2013**, *52*, 5033 – 5036; c) M. R. Golder, B. M. Wong, R. Jasti, *Chem. Sci.* **2013**, *4*, 4285 – 4291.

[12] a) H. Takaba, H. Omachi, Y. Yamamoto, J. Bouffard, K. Itami, *Angew. Chem.* **2009**, *121*, 6228 – 6232; *Angew. Chem. Int. Ed.* **2009**, *48*, 6112 – 6116; b) Y. Segawa, S. Miyamoto, H. Omachi, S. Matsuura, P. Senel, T. Sasamori, N. Tokitoh, K. Itami, *Angew. Chem.* **2011**, *123*, 3302 – 3306; *Angew. Chem. Int. Ed.* **2011**, *50*, 3244 – 3248; c) H. Omachi, S. Segawa, K. Itami, *Acc. Chem. Res.* **2012**, *45*, 1378 – 1389; d) C. Camacho, T. A. Niehaus, K. Itami, S. Irle, *Chem. Sci.* **2013**, *4*, 187 – 195.

[13] B. M. Wong, *J. Phys. Chem. C* **2009**, *113*, 21921 – 21927.

[14] T. Iwamoto, Y. Watanabe, Y. Sakamoto, T. Suzuki, S. Yamago, *J. Am. Chem. Soc.* **2011**, *133*, 8354 – 8361.

[15] S. Huang, A.-M. Ren, J.-F. Guo, X.-T. Liu, J.-K. Feng, *Polymer* **2012**, *53*, 2991 – 3000.

[16] S. Anderson, H. L. Anderson, J. K. M. Sanders, *Acc. Chem. Res.* **1993**, *26*, 469 – 475.

[17] a) T. R. Kelly, L. R. Xie, C. K. Weinreb, T. A. Bregant, *Tetrahedron Lett.* **1998**, *39*, 3675 – 3678; b) C. A. Hunter, S. Tomas, *J. Am. Chem. Soc.* **2006**, *128*, 8975 – 8979; c) J. S. Lindsey, *New J. Chem.* **1991**, *15*, 153 – 180.

[18] Y. Cohen, L. Avram, L. Frish, *Angew. Chem.* **2005**, *117*, 524 – 560; *Angew. Chem. Int. Ed.* **2005**, *44*, 520 – 554.

[19] D. M. Tiede, R. Zhang, L. X. Chen, L. Yu, J. S. Lindsey, *J. Am. Chem. Soc.* **2004**, *126*, 14054 – 14062.

[20] R. F. Kelley, S. J. Lee, T. M. Wilson, Y. Nakamura, D. M. Tiede, A. Osuka, J. T. Hupp, M. R. Wasielewski, *J. Am. Chem. Soc.* **2008**, *130*, 4277 – 4284.

[21] P. V. Konarev, V. V. Volkov, A. V. Sokolova, M. H. J. Koch, D. I. Svergun, *J. Appl. Crystallogr.* **2003**, *36*, 1277 – 1282.

[22] Single-crystal X-ray diffraction data were collected by using beamline I19 (EH1) at Diamond Light Source [H. Nowell, S. A. Barnett, K. E. Christenden, J. S. Teat, D. R. Allen, *J. Synchrotron Radiat.* **2012**, *19*, 435 – 441]. The structure was solved using SuperFlip [L. Palatinus, G. Chapuis, *J. Appl. Crystallogr.* **2007**, *40*, 786 – 790], which identified the heavy atom positions as well as some fragments of the light atoms structure (Figure S5) and indicated the space group was *Cc*. This structure was developed by using a mixture of difference Fourier methods and structure

modeling techniques interspersed with cycles of least-squares refinement with shift-limiting restraints to stabilize the optimization within CRYSTALS [P. W. Betteridge, J. R. Carruthers, R. I. Cooper, K. Prout, D. J. Watkin, *J. Appl. Crystallogr.* **2003**, *36*, 1487]. The atomic skeleton of the model exhibited C_2 symmetry about the center, where the acetylene bridges cross. The presence of this molecular symmetry within the space group *Cc* suggested that symmetry had been omitted. Close examination of the position of the C_2 operator with respect to the remaining structure suggested the correct space group was actually the far more abundant *C2/c*. The model was transformed to give half a molecule in the asymmetric unit. Once the model was complete, further examination of the difference map indicated the presence of diffuse electron density was due to disordered solvent. Hydrogen atoms were placed at geometric positions [R. I. Cooper, A. L. Thompson, D. J. Watkin, *J. Appl. Crystallogr.* **2010**, *43*, 1100 – 1107] and PLATON/SQUEEZE [A. L. Spek, *J. Appl. Crystallogr.* **2003**, *36*, 7 – 13; P. van der Sluis, A. L. Spek, *Acta Crystallogr., Sect. A: Found. Crystallogr.* **1990**, *46*, 194 – 201] was applied. To maintain a sensible geometry, copious restraints were necessary. In general, rather than restraining bond lengths and angles to absolute values, "SAME" restraints were used extensively making use of the repeated porphyrin motif and its symmetry. Extensive use was also made of thermal similarity and vibrational restraints to allow the displacement parameters to adopt slightly aspherical geometry while ensuring they remained sensible. Best efforts were made to remove the geometric restraints, however, it was necessary to leave a considerable number in the final refinement keeping the final model consistent with results from the related structure of the six-porphyrin nanoring. For further details, see the Supporting Information and CIF file.

[23] S. M. Curtis, N. Le, F. W. Fowler, J. W. Lauher, *Cryst. Growth Des.* **2005**, *5*, 2313 – 2314.

[24] T. Steiner, *Angew. Chem.* **2002**, *114*, 50 – 80; *Angew. Chem. Int. Ed.* **2002**, *41*, 48 – 76.

[25] a) M. Nishio, *Phys. Chem. Chem. Phys.* **2011**, *13*, 13873 – 13900; b) S. Tsuzuki, A. Fujii, *Phys. Chem. Chem. Phys.* **2008**, *10*, 2584 – 2594.

[26] A. Saywell, J. K. Sprafke, L. J. Esdaile, A. J. Britton, A. Rienzo, H. L. Anderson, J. N. O'Shea, P. H. Beton, *Angew. Chem.* **2010**, *122*, 9322 – 9325; *Angew. Chem. Int. Ed.* **2010**, *49*, 9136 – 9139.

[27] H. J. Hogben, J. K. Sprafke, M. Hoffmann, M. Pawlicki, H. L. Anderson, *J. Am. Chem. Soc.* **2011**, *133*, 20962 – 20969.

Received: May 28, 2014
Published online on August 25, 2014

